IECEC2001-CT-41

FABRICATION AND USE OF PARALLEL PLATE REGENERATORS IN THERMOACOUSTIC ENGINES
LAUR–01-1393

S. Backhaus and G. W. Swift
Condensed Matter and Thermal Physics Group
Los Alamos National Laboratory
Los Alamos, NM 87545

ABSTRACT

Diagnostic and performance measurements on a thermoacoustic-Stirling heat engine (TASHE) utilizing a parallel-plate regenerator are presented. The diagnostic measurements demonstrate that the spacing between the regenerator plates is very uniform and close to the design spacing of 102 μm. Achieving a high degree of uniformity, which is crucial to the regenerator performance, requires careful fabrication. The details of this process are described. The performance measurements show that the viscous losses in the regenerator are quantitatively understood while unforeseen heat leaks show that the heat transfer properties are only qualitatively understood. By switching from a screen-based regenerator to a parallel-plate regenerator, the power output of the TASHE was nearly doubled with a significant increase in efficiency at the highest acoustic power output.

INTRODUCTION

Regenerators in Stirling or Stirling-like machines are designed to provide sufficient thermal contact to the working gas to minimize loss due to irreversible heat transfer while generating as little viscous loss as possible. Theoretically, parallel-plate regenerators offer a significant performance advantage over screen-based regenerators. In comparing these two types of regenerators, it is useful to look at the ratio $StPr^{2/3}/f$ where St and Pr are the Stanton and Prandtl numbers respectively and f is the friction factor[1]. This ratio becomes larger as heat transfer improves or viscous loss decreases. For steady laminar flow through parallel plates, this ratio is ~0.4 and is independent of Reynolds number. For screen beds with properties typical of Stirling machines and even at a Reynolds number of ~20, this ratio is ~0.1. This difference provides a strong motivation to use the parallel-plate geometry in Stirling regenerators.

However, small variations of the plate spacing can negate any gains from the change of geometry. The viscous flow resistance in the gap between two parallel plates is $\propto 1/h^3$ where h is the plate spacing. Typically h is around 100 μm in engines and 25 μm or smaller in cyrogenic refrigerators. Therefore, variations in h on the order of 10 μm from channel to channel lead to ~30% variations in the flow resistance in an engine and >200% variations in a refrigerator. In a parallel-plate regenerator with flow-channel gaps distributed about some average gap, the wider gaps will garner more of the flow per cross-sectional area than the narrow gaps. In addition, the thermal contact between the gas in the gaps and the plates falls off as 1/h. Therefore, the gaps with the poorest thermal contact have to handle the majority of the heat transfer. This leads to high thermal losses.

Over the past few years, we have developed a thermoacoustic-Stirling heat engine (TASHE) that generates in-phase pressure and velocity oscillations in a regenerator and, therefore, utilizes a Stirling-like thermodynamic cycle[2]. The engine resembles a "gamma-style" Stirling engine where the dynamic properties of the displacer piston are achieved by the inertia of the gas in an "inertance" tube, and the thermal-insulation properties of the displacer piston are achieved by thermally stratified gas motion in a "thermal buffer" tube. Also, the power piston is replaced by the inertia of the gas in an acoustical resonator attached to the TASHE and by deliberate dissipation in a variable acoustic load impedance. We will not describe the TASHE in detail here, but instead refer the reader to Ref. [2]. Recently, we have replaced the TASHE's screen-based regenerator with a parallel-plate regenerator. This article reports on the fabrication and testing of the regenerator as well as the performance of the TASHE while using it.

REGENERATOR FABRICATION

The completed parallel-plate regenerator is a cylinder 88.9 mm in diameter and 73.0-mm long. It is constructed from a

stack of alternating stainless-steel sheets shown in Fig. 1; 1,500 sheets are required to complete the regenerator. Both sheet A and sheet B are fabricated by photochemical milling (PCM) of 316L stainless-steel sheet. This alloy was chosen because of its availability and good diffusion bonding properties. Other, lower thermal conductivity metals, such as Inconel 625, could have been used. Sheet A, which is 104-μm thick, has 1.02-mm-wide by 73-mm-long windows etched through it. The windows are spaced 1.27 mm on-center leaving 0.25-mm-wide fingers separating the windows. Along their long dimension, which is also the flow direction, the windows are interrupted at either end and in the middle by 0.25-mm-wide webs that are etched approximately half-way through, i.e. 52-μm deep. The webs provide lateral support for the extremely long, thin fingers, and the half etches provide spacing for the oscillatory flow to enter and exit the windows as well as cross over the middle web. Sheet B, which is 25-μm thick, has 1.02-mm square holes etched though it. When stacked above and below Sheet A, the square holes are centered over the middle set of webs on Sheet A and provide additional area for the flow to cross over the middle web. In a trial PCM run, square notches were also etched at the edges of Sheet B to provide additional room for the entering and exiting flow, but these features made the edges of Sheet B jagged, extremely delicate, and difficult to handle.

Figure 2 shows Section CC, a cross section perpendicular to the flow direction. Sheet B forms the two long walls of many 1.02-mm wide by 104-μm high flow channels. The 1.02-mm width of the channels is set by the width of the PCM'd windows in Sheet A. The crucial, 104-μm height dimension is determined by the accurately rolled thickness of Sheet A. When the A sheets were received from the PCM manufacturer, the variation of the unetched thickness from sheet to sheet and along any one sheet was less than 3 μm. The B sheets showed similar small variations. However, the half-etched regions in the A sheets, shown in Section DD, showed wide variations. On some A sheets, the webs were etched completely through. On others, the half-etched region was 81-μm thick, i.e. only 23 μm etched away.

This wide variation in the half-etch thickness is the main reason why half-etching should not be used to set the important dimensions of the flow channels in a parallel-plate regenerator.

After the PCM process is complete, the next steps are cleaning, sorting, stacking, and diffusion bonding of the stacked sheets. The PCM process is performed on "parent sheets" that contain 9 of the A or B sheets. The cleaning is done before removing the A and B sheets from the parent. For the B sheets, a dilute nitric-acid etch is followed by a de-ionized water rinse and then an isopropyl-alcohol rinse. Then, the sheets are dried with a heat gun. The A sheets are too delicate to clean in this manner. Water spots are removed with isopropyl alcohol and a cotton swab. Following this, any handling of the sheets is done while wearing latex gloves.
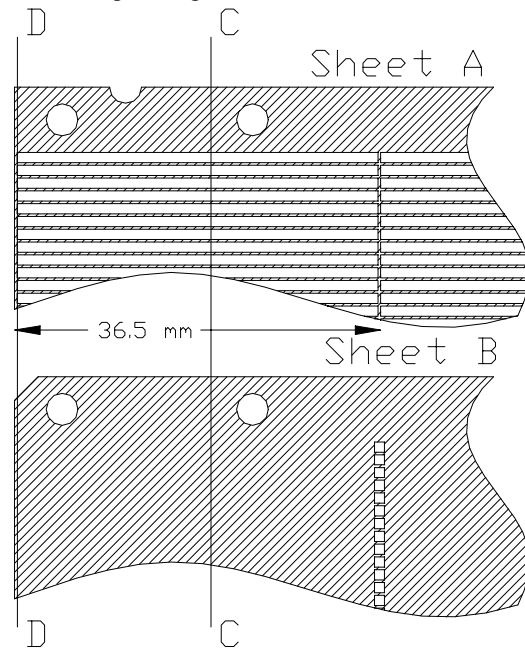
Figure 1. Plan view of the upper left corner of Sheet A and Sheet B. The oscillating flow is from left to right. The hole in Sheet A near the middle web is used to ensure all the A sheets are stacked with the half-etched side up. The area near the top of Sheet A and B is used only for the alignment holes. It is machined away later in the fabrication. Except for the extra hole mentioned above, the sheets are symmetric about the horizontal and vertical centerlines.

During the PCM process, a 0.25- to 0.50-mm gap is etched through around the perimeter of the sheets except in four locations where thin tabs hold the individual sheets in the parent sheet. The individual sheets are removed by cutting the tabs with either a razor blade or surgical scissors. During removal, the individual sheets are sorted into "good," "useable," and "rejects." Rejects include A sheets with torn or etched through webs, A sheets with bent fingers, sheets with incompletely etched windows, or sheets with excessive water spotting. Moderate bends in the A-sheet fingers, which looked like they could be straightened, were deemed "useable." As required to complete the full stacking height, the "usable" sheets were repaired.

An additional detail in the PCM process eases the removal and later stacking of the individual sheets. When cutting the tabs on Sheet B, burrs are raised that would interfere with the stacking. Half circles are etched in Sheet A that, when interleaved with Sheet B, are aligned with the burrs on Sheet B and provide clearance for them. The corners of Sheet B are etched away for a similar reason. Without these details shown in Fig. 1, the burrs would have to be cut flush with the sheets.
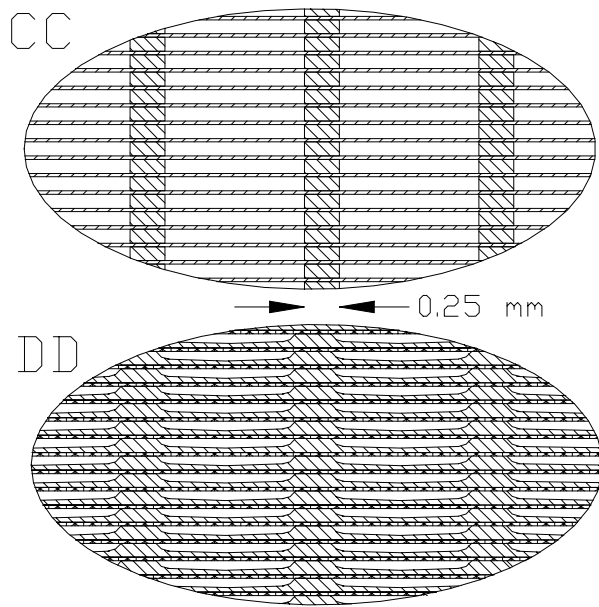
Figure 2. Enlarged view of Sections CC and DD after stacking alternating Sheets A and B. The oscillating flow is into and out of the page. In CC, the rectangular fingers of Sheet A are 104-μm high by 0.25-mm wide. In DD, the half-etched webs of Sheet A are shown. Although they are drawn as if they are very uniform, the half-etch depths show wide variation.

The sheets are then stacked onto a thick 316L plate that holds four 316L registration pins to align the sheets. The pins fit snugly into PCM'd holes near the corners of the individual sheets. Although the registration pins hold the perimeters of the sheets in excellent alignment, the delicate half-etched webs in the A Sheets are often slightly distorted from handling of the sheets leading to misalignment of several of the fingers. Later in the fabrication process, misalignment of a finger would lead to buckling around the misaligned finger and many nearby fingers, resulting in collapsed or irregular flow channels. Therefore, the fingers must be inspected and their alignment individually corrected during the stacking. One technique that was found useful involves stacking up many tens of the sheets on a separate fixture, using a pointed scalpel to align the fingers under a low-power microscope, transferring the short stack onto the main stack, and realigning the interface layers under the microscope. After a sufficient stack height is achieved (95 mm in this case, allowing for machining waste and plastic strain generated during the diffusion bond), a second thick 316L plate is added to the top of the stack.

Next, the stack is vacuum hot pressed by standard techniques[3] to form a diffusion bond between the layers. After fabrication, the regenerator will not be subject to large stresses, so bond strength is not crucial. Avoiding buckling of the 95-mm-high, 0.25-mm-wide columns shown in Fig. 2 is of the highest importance. The Euler formula gives the buckling stress as[4] $\sigma_b = C\pi^2 E/(L/r)^2$ where E~18x10^6 psi is the elastic modulus at the bonding temperature, L is the 95-mm height of the stack, and r is the smallest radius of gyration of the column (~0.289 W, where W is the 0.25-mm width of a single column). Also, C is a constant between 1 and 4 that depends on the condition at the ends of the column. It should be taken as 1 for a conservative estimate of the buckling stress. During the vacuum hot pressing of this regenerator, the largest applied load never exceeded ½ of the estimated buckling stress. Also, the temperature was ramped up to and down from the bonding temperature slowly to avoid temperature differences between the interior and exterior of the part. Large temperature differences generate large thermal stresses, which would distort the freestanding sections of the B sheets. A post-bond visual inspection of the regenerator showed no buckling of the columns due to overloading or misalignment and no distortion of the B sheets. Also, the interlayer bonds were found to be of sufficient strength.

The bonded stack of sheets is then machined[5] into a cylinder by electric discharge machining (EDM). Within one flow-channel width around the cut, the EDM process distorts the B sheets considerably. For this reason, cuts perpendicular to the flow direction should be minimized. Only clean water should be used during the EDM process and the faces of the regenerator should be masked to minimize the amount of EDM "dust" left inside the flow channels. The resulting cylinder is then pressed into a thin-walled stainless-steel sleeve (0.5-mm wall) to protect it from damage and ease its installation and removal from the TASHE. To obtain a tight fit between the regenerator and the sleeve, the I.D. of the sleeve is machined a few thousandths of an inch undersize and heated while the regenerator is pressed into place. The regenerator should not be "shrunk-fit" into the sleeve, because the thermal shock to the regenerator might distort the freestanding B sheets. To remove any EDM dust that may have been introduced into the flow channels, the regenerator is filled with isopropyl alcohol (surface tension holds the alcohol in the channels), which is then blown out with dry nitrogen. This process is repeated until the alcohol runs out clean. EDM distortion of the flow channels around the O.D. of the regenerator is too severe to allow those channels to be accessed by the oscillating flow in the TASHE. Therefore, the outer layer of channels is blocked at the cold end of the regenerator using Stycast 2850 epoxy. The fractional loss of flow area is only ~4% in a regenerator with this large diameter.

DIAGNOSTIC MEASUREMENTS

Visual inspection of the ends of the completed regenerator (Section DD) shows that the B sheets remained flat and parallel, at least at the ends of the regenerator. A steady-flow pressure-drop test is performed to quantify the uniformity and dimensions of the channels.

Copyright © #### by ASME

To measure the steady-flow pressure drop, the regenerator is sealed into a metal housing using O-rings to ensure no flow can pass around the outside of the regenerator sleeve. The housing is glued to a 1.8-m-long entrance section and a 0.6-m-long exit section. Both are made from PVC pipe with an I.D. slightly larger than the regenerator O.D. A copper screen flow straightener is placed 1 cm from the entrance side of the regenerator. The exit from the test section leads into a 0.8-m-long pipe, which houses a Laminar Flow Element[6] (LFE) used to measure the flow rate. Room temperature, atmospheric pressure, dry argon is supplied at the end cap of the entrance. The temperature of the argon is measured with a type-K thermocouple located between the flow straightener and the regenerator. The pressure drops across the regenerator and LFE are measured with two differential, Bourdon-tube pressure gauges. The LFE and the two pressure gauges are calibrated to NIST-traceable standards.
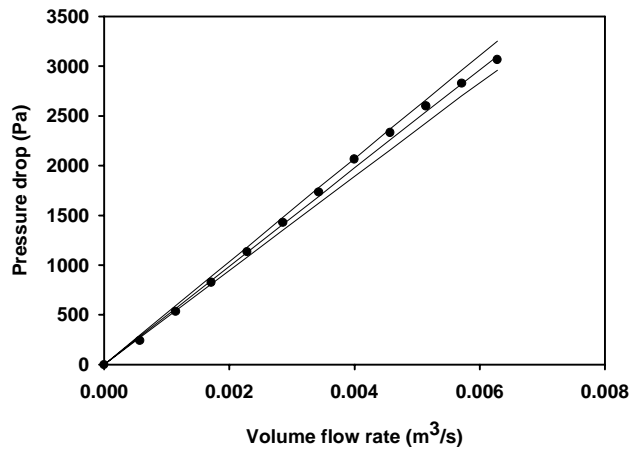

Figure 3. Pressure drop across the parallel-plate regenerator due to steady flow. The circles are the measured data and the upper, middle, and lower lines are the calculated pressure drops for channel heights of 102, 104, and 107 μm respectively.

The pressure drop across the regenerator is measured for flow rates up to 0.007 m³/s, i.e. 1.7 m/s in the channels. The results are shown as the circles in Fig. 3. For the channel height of 104 μm and width of 1.02 mm, this corresponds to a Reynolds number based on hydraulic diameter Re_{Dh}=18. At this low Reynolds number, the flow in the regenerator is laminar. Also, entrance and exit pressure losses at the ends and middle of the regenerator are estimated to be small. Therefore, the total pressure drop can be calculated from the laminar friction factor[1]. The pressure drop at the ends and middle, where the geometry changes due to the half-etched webs, is calculated assuming the flow in these short regions to be laminar and fully developed. These three short sections contribute about 5% of the total pressure drop, so this assumption should not significantly affect the calculation of the total pressure drop. The measurements are in closest agreement

with a 104-μm channel height, which is the average measured thickness of the A sheets. This result, coupled with the visual inspection of the regenerator, leads us to believe the flow channels are uniform and parallel to about 3 μm.

PERFORMANCE MEASUREMENTS

When we are satisfied that we built what we intended, the regenerator is installed into the TASHE. A complete set of performance measurements is taken in a similar fashion to those reported for the TASHE operating with a screen-based regenerator[2]. In summary, heat is supplied to the hot end of the regenerator by an electric resistance heater, and waste heat is removed from the cold end of the regenerator by water flowing through a shell-and-tube heat exchanger. The power produced by the TASHE, and delivered to the resonator and variable acoustic load, is measured near the resonator entrance. Here, we report on measurements specific to the regenerator.
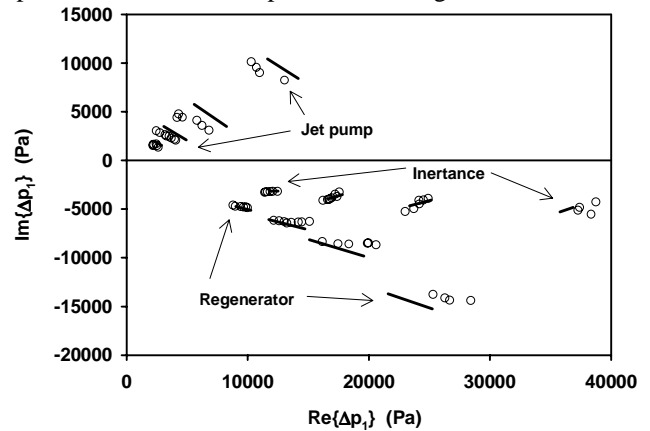

Figure 4. Measured and numerically calculated pressure-drop phasors across the feedback inertance, jet pump, and regenerator. Data are taken at fixed values of $p_{1,c}/p_m$ equal to 0.038, 0.051, 0.069, and 0.10. For the different pressure drops, $p_{1,c}/p_m$ is higher for the data farther from the origin. At each $p_{1,c}/p_m$, T_h is swept from the minimum T_h required to reach that amplitude to a maximum of 725°C by adjusting the variable acoustic load on the TASHE.

With the geometry of the parallel-plate regenerator confirmed by visual inspection and flow testing, the oscillatory pressure drops in the TASHE are measured to confirm our understanding of the acoustic field inside the TASHE. If the pressure drops across the various elements in the loop of the TASHE agree with numerical calculations[7], then the numerical code is making reasonably accurate predictions of the volumetric-flow-rate phasors throughout the TASHE. Figure 4 shows the measured and calculated pressure-drop phasors across the feedback inertance, jet pump, and regenerator. The various groups of data points (open circles) are taken at fixed $p_{1,c}/p_m$ while T_h is varied from the minimum value at which the engine runs at $p_{1,c}/p_m$ to a maximum of 725°C. The solid lines connect the calculated values of the pressure-drop phasors at the lowest and highest T_h for each value of $p_{1,c}/p_m$. Here, p_m is

the mean pressure of helium gas (450 psia) inside the TAHSE, $p_{1,c}$ is peak oscillating pressure amplitude measured at the cold end of the regenerator, and T_h is the temperature of the regenerator sleeve at the hot end of the regenerator. For this and all subsequent data, the temperature at the cold end of the regenerator, T_c, is between 20°C and 60°C. At low values of $p_{1,c}/p_m$ the measured pressure-drop phasors are in good agreement with the calculations. At higher $p_{1,c}/p_m$, the ~10% discrepancies are due mainly to our limited knowledge of the acoustic impedance of the jet pump[2].

With some confidence in the numerical predictions of the volumetric-flow-rate phasors, the measured acoustic power flow and heat flows are compared with the numerical predictions. Figure 5 shows the acoustic power flow into the resonator generated by the TASHE for the same values of $p_{1,c}/p_m$ as in Fig. 4. The numerical calculation is in excellent agreement with the data, confirming our understanding of the TASHE acoustics, volumetric flow rates, and the regenerator pressure-drop properties. Also, the acoustic power output of the TASHE utilizing this parallel-plate regenerator is nearly twice that achieved with a screen-based regenerator[2].
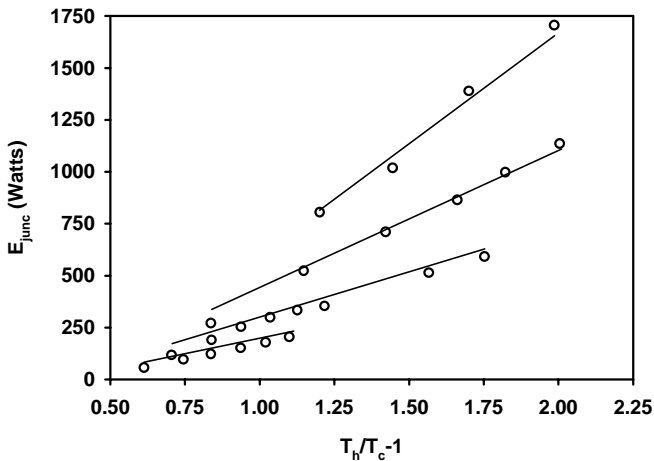

Figure 5. Open circles, measured acoustic power flow into the resonator, E_{junc}, generated by the TASHE. $p_{1,c}/p_m$ is higher for the larger power flows. Acoustic power is measured using a two-microphone technique[8]. For each value of $p_{1,c}/p_m$, E_{junc} is calculated at the highest and lowest value of T_h/T_c-1. The lines connect these values.

An additional data run is taken with the acoustic load set so that the engine will not oscillate even with T_h~725°C. By measuring the heat input to the hot heat exchanger, Q_h, and the heats rejected at the main cold heat exchanger, $Q_{c,1}$, and the secondary cold heat exchanger, $Q_{c,2}$, the heat leaks through the various components are determined. This is described in more detail in Ref. [2]. These heat leaks are included in the numerical model of the TASHE.
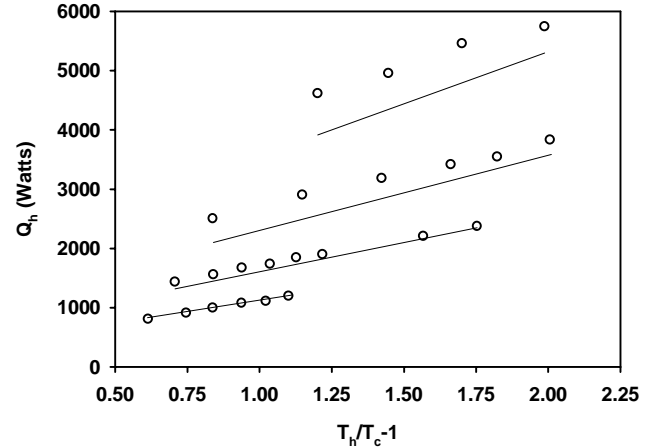

Figure 6. Open circles, measured heat absorbed at the hot heat exchanger vs. T_h/T_c-1 for the same values of $p_{1,c}/p_m$ as in Fig. 4. Higher values of $p_{1,c}/p_m$ correspond to larger Q_h. Q_h is determined by measuring the electric power flowing into the electrically-heated hot heat exchanger. For each $p_{1,c}/p_m$, Q_h is calculated at the highest and lowest values of T_h/T_c-1. The lines connect these calculated values.
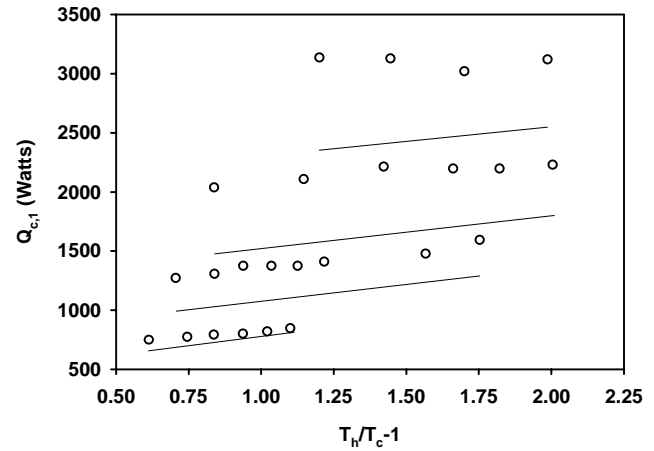

Figure 7. Open circles, measured heat rejected at the main cold heat exchanger vs. T_h/T_c-1 for the same values of $p_{1,c}/p_m$ as in Fig. 4. Higher values of $p_{1,c}/p_m$ correspond to larger $Q_{c,1}$. $Q_{c,1}$ is determined by measuring both the flow rate of cooling water through the main cold heat exchanger and the temperature drop across it. For each $p_{1,c}/p_m$, $Q_{c,1}$ is calculated at the highest and lowest values of T_h/T_c-1. The lines connect these calculated values.

The measured and calculated heat flows Q_h and $Q_{c,1}$ are shown in Figs. 6 and 7. At higher values of $p_{1,c}/p_m$, the measured Q_h is significantly higher than the calculated values. The discrepancy in $Q_{c,1}$ is approximately the same as Q_h. This implies that the extra heat the engine is absorbing at the hot heat exchanger is being rejected at the main cold heat exchanger. There is also a discrepancy between the measured and calculated $Q_{c,2}$, but it is much smaller than the difference in $Q_{c,1}$. All conduction and radiation heat leaks are accounted for by the

heat leak measurements. Therefore, the extra heat must be carried by the oscillating gas itself.

One clue to the mysterious heat-transport mechanism is the axial temperature profile in the regenerator. When using the screen-based regenerator[2], the temperature always varied linearly from the cold exchanger to the hot exchanger, i.e. the temperature measured at the axial midpoint of the regenerator was always within a few percent of the average of T_h and T_c. However, the temperature at the axial midpoint of the circumference of the parallel-plate regenerator typically runs 15 to 20% hotter than the average of T_h and T_c. This temperature distribution cannot be explained by either the numerical model or the temperature dependence of the thermal conductivity of the metals used in the regenerator and its pressure vessel. One effect that is known to cause both a temperature distribution that deviates from linear and extra heat transport is a steady flow of gas around the loop of the TASHE, here called streaming[2]. However, streaming around the entire loop would also cause the axial temperature distribution in the buffer tube to deviate from linear. This is not observed. Another possibility is a circulating acoustic streaming loop contained entirely within the regenerator similar to that observed in the pulse tubes of orifice pulse tube refrigerators[9]. The streaming might be driven by the same mechanisms that cause the circulating streaming in pulse tubes or by small, undetected variations in the regenerator plate spacing. Four thermocouples placed around the O.D. of the regenerator sleeve indicate that the axial midpoint temperature does not show a significant angular dependence. Therefore, whatever the mechanism, it must be occurring on a single or few-channel scale.
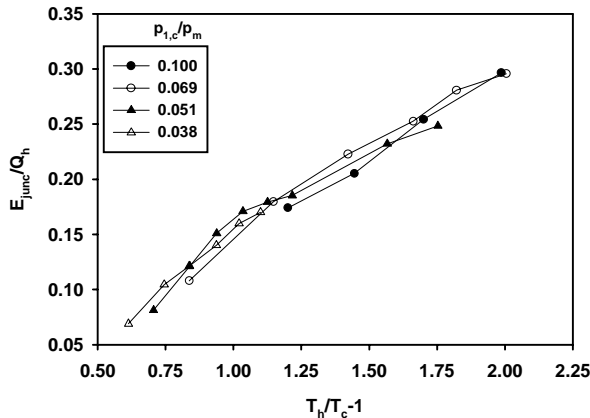
Figure 8. Measured thermal efficiency of the TASHE vs. T_h/T_c-1 for the same values of $p_{1,c}/p_m$ as in Fig. 4.

In spite of the mysterious extra heat leak from the hot heat exchanger and the high thermal conductance of the 316L fingers, the measured TASHE efficiency with a parallel-plate regenerator shown in Fig. 8 is still quite good. By switching from a screen-based to a parallel-plate regenerator, the acoustic power output of the TASHE is nearly doubled with no decrease in maximum efficiency[2]. In fact, the efficiency at $p_{1,c}/p_m$=0.10 has increased from 22% to 30%. This is mainly due to the flow

resistance of the parallel-plate regenerator remaining linear at this amplitude whereas the screen-based regenerator shows significant nonlinear behavior at the higher amplitudes.

CONCLUSIONS

If they are constructed with care and carefully inspected after fabrication, parallel-plate regenerators offer significant advantages over screen-based regenerators. We have attempted to define a procedure for the fabrication and diagnostic testing of parallel-plate regenerators. We have demonstrated that, by following this procedure, the viscous pressure drop of the regenerator is very close to that given by theoretical calculations. This shows that the plate spacing is very uniform and close to the design spacing. However, the heat transfer properties are only qualitatively understood. A small but significant extra source of heat transport through the regenerator exists. The experimental evidence points towards streaming as the source of this heat transport, but the precise mechanism driving the transport remains unknown.

REFERENCES

[1] W. M. Kays and A. L. London, Compact Heat Exchangers, 3rd edition (McGraw-Hill, New York, 1984).

[2] S. Backhaus and G. W. Swift, "A thermoacoustic-Stirling heat engine-Detailed study," J. Acoust. Soc. Am., **107** (6), 3148-3166, (2000).

[3] Refrac Systems, Inc. 7201 W. Oakland St., Chandler, AZ.

[4] R. J. Roark and W. C. Young, Formulas for Stress and Strain, 5th edition (McGraw-Hill, New York, 1975). pg. 415.

[5] Micro-Tronics, Inc. 2905 S. Potter Dr., Tempe, AZ.

[6] Meriam Instrument, 10920 Madison Ave., Cleveland, OH.

[7] W. C. Ward and G. W. Swift, "Design environment for low amplitude thermoacoustic engines (DeltaE)," J Acoust. Soc. Am., **95**, 3671-3672 (1994). To review or obtain DeltaE, visit http://www.lanl.gov/projects/thermoacoustics.

[8] A. M. Fusco, W. C. Ward, and G. W. Swift, "Two-sensor power measurements in lossy ducts," J. Acoust. Soc. Am. **91**, 2229-2235 (1992).

[9] J. M. Lee, P. Kittel, K. D. Timmerhaus and R. Radebaugh, "Flow patterns intrinsic to the pulse tube refrigerator." In Proc. 7th Int. Cryocooler Conf., Kirtland AFB, NM 87117-5776, Phillips Laboratory, 1993, p. 125.